Macromolecules

pubs.acs.org/Macromolecules Article

Relating the Degree of Nanofiller Functionality to the Glass Transition Temperature and Structure in a Polymer–Polyhedral Oligomeric Silsesquioxane Nanocomposite

Walter W. Young, Rui Shi, Xiang-Meng Jia, Hu-Jun Qian,* and Reika Katsumata*

Cite This: *Macromolecules* 2022, 55, 4891–4898 Read Online

ACCESS | Metrics & More | Article Recommendations | Supporting Information

ABSTRACT: Surface interactions between a polymer and filler dictate the properties of polymer nanocomposites, yet molecular-level understanding remains a challenge. Here, we show that the glass transition temperature (T_g) of a polymer nanocomposite composed of poly(2-vinylpyridine) and polyhedral oligomeric silsesquioxanes (POSSs) with a variable number of hydrogen bond-donating amines is well explained by the product of the number of interaction sites (n_{amine}) and the POSS volume fraction (ϕ_{POSS}). The glass transition temperature of the nanocomposites found by coarse-grained simulations agrees reasonably well with experimental results of differential scanning calorimetry, indicating that the excess interaction energy from hydrogen bonds is responsible for the change in T_g in the system. All-atom molecular dynamics simulations reveal that the number of hydrogen bonds is approximately proportional to n_{amine}, though the amines on POSSs with lower n_{amine} are able to form slightly more hydrogen bonds than POSSs with higher n_{amine} due to geometric frustrations of polymers bonding to two adjacent bond donors. Expanding this atomic perspective to other polymer nanocomposites could lead to advancements in materials development.

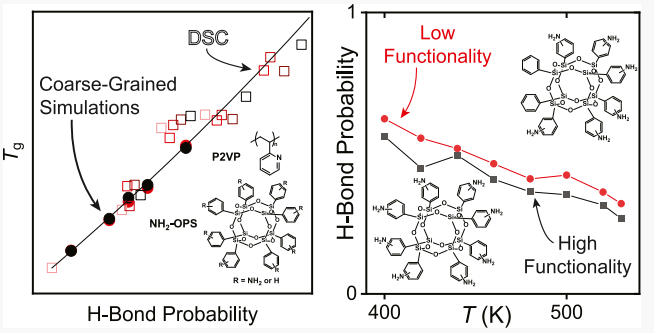

INTRODUCTION

Polymer nanocomposites, a soft polymer material loaded with a hard nanoscopic filler, are interesting for their ability to access properties otherwise unattainable in either soft or hard materials alone.[1] However, rationalizing and understanding this property enhancement remains challenging, though it is clear that factors such as surface interactions,[2−12] the nanofiller size,[13−18] polymer chain stiffness,[2] and even processing conditions[1,3,19] are of critical importance for developing design rules and fundamental models for these materials. In particular, when nanofillers are small enough to be considered dispersed on the molecular scale, the effects of the filler can differ dramatically from those of larger (∼10 nm) fillers.[12,14−16]

Polyhedral oligomeric silsesquioxanes (POSSs), well-defined silicone structures with the general chemical formula $(R\text{-}SiO_{1.5})_n$, are particularly useful fillers for achieving massive property enhancements due to higher polymer–filler interfacial areas. The precise hybrid organic–inorganic structure of POSSs allows for atomic-level precision in chemistry and formulation, thus allowing atomic-level insights otherwise unattainable in systems with larger, less well-defined fillers. These molecularly dispersed nanocomposites typically remain processable due to the lack of rheological jamming in the terminal flow regime[7,14,15,20,21] and can exhibit substantial enhancement in gas barrier properties[20] and glass transition temperature (T_g).[7,14,15]

The glass transition temperature is among the most important physical properties of polymers as the difference between the operating temperature and T_g determines the suitability of polymers and their composites in applications. Though the effects of POSS loading on polymer T_g are extensively studied, a general understanding of this behavior which accounts for the composition of the polymer and POSS has only recently begun to emerge.[7,22] Polymer/POSS nanocomposites have shown a variety of effects on T_g, including the broadening of the transition region[14] and either enhancement or suppression of T_g, depending on the chemical structure of the polymer and POSS.[7,22] In strongly interacting systems, polymer–POSS interactions can increase T_g up to 35 K,[7,14] while some POSS fillers can also greatly reduce T_g as much as ∼100 K by increasing the free volume, despite the presence of strong polymer–POSS interactions.[23,24] Our recent work has suggested that this effect can be fitted with the Fox equation[25] by considering fractions of "bonded" and "unbonded" monomers, but the effect of POSS composition

Received: March 29, 2022
Revised: May 18, 2022
Published: June 7, 2022

https://doi.org/10.1021/acs.macromol.2c00646
Macromolecules 2022, 55, 4891–4898

on glass transition temperatures remains relatively unexplored.[7] Previous experiments and simulations of analogous systems (nanocomposites and thin films) showed T_g enhancement in nanoconfined polymers, with an approximately linear increase in T_g with interaction strength.[26−31] This can be treated quantitatively with various theories of glass formation, with interaction strength being modeled as a cohesive energy density,[32] work of adhesion,[31] or sticker fraction in neat linear polymers with attractive endgroups.[33]

However, not all nanocomposites display this strong dependence of interaction strength on T_g as many polymer nanocomposite systems will form an interfacial layer of relatively immobile polymer chains which do not participate in the glass formation of the free chains.[34] In one example, a poly(2-vinylpyridine) (P2VP)/silica composite with fillers on the order of ∼10 nm was modified by capping some of the siloxane groups to vary the polymer−filler interaction strength, but no strong trend of T_g with interaction strength was observed.[6] Thus, nanocomposites created with POSS fillers offer a unique perspective as high interfacial attraction can be achieved with a nearly uniform distribution of the interfacial surface area in the polymer matrix.

In this work, we conduct simulations and experiments to study the effect of POSS surface chemistry on T_g of P2VP composites by precisely tuning n_{amine}, the number of amines (hydrogen bond donors), present on POSS, that is, variably aminated octa(phenyl) silsesquioxane (NH_2-OPS) (Figure 1). Coarse-grained simulations demonstrate that the T_g enhancement is primarily caused by excess energy of interaction between the filler and matrix. In these simulations, we abstract POSS by a core−shell model, effectively decorated with six or eight amine sites on the surface in the P2VP matrix. The T_g of the nanocomposite and the excess hydrogen bond energy are found to be linear with the total number of amine groups on NH_2-OPS. To create nanocomposites for differential scanning calorimetry (DSC) experiments, NH_2-OPS is synthesized according to literature procedures and loaded into P2VP (Figure 1a).[35] Our results from coarse-grained simulations and DSC show that T_g increases with the number of interaction pairs present in the system.

To provide a molecular picture of the polymer−POSS interactions, the number of hydrogen bonds present in the system is studied by all-atom molecular dynamics simulations (Figure 1b).[12] We observe a strong temperature dependence of hydrogen bonding in the nanocomposites and also that NH_2-OPS with fewer hydrogen bond-donating amines will form slightly more hydrogen bonds per amine than a fully functionalized NH_2-OPS. This demonstrates that the assumption of random mixing of monomers and nanofillers is an approximation. Overall, our results suggest that the number of interactions is a robust framework for understanding the T_g of a polymer/POSS nanocomposite and highlight the importance of molecular-scale geometry and size effects.

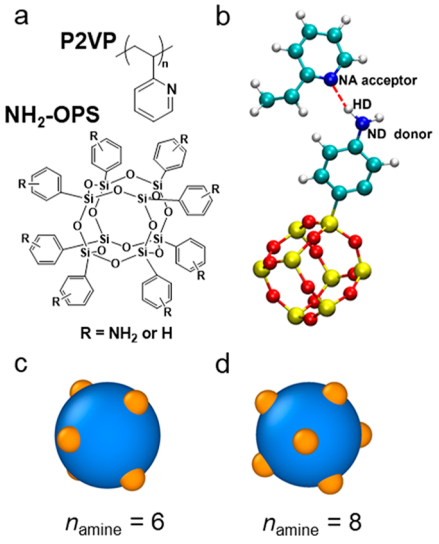

Figure 1. (a) General chemical structures of NH_2-OPS and P2VP. (b) Illustration of a hydrogen bond formed between NH_2-OPS and pyridine on the P2VP matrix from all-atom molecular dynamics simulations. For clarity, only one NH_2-OPS side group and one 2-vinyl pyridine unit are shown. The hydrogen bond N···−H−N is formed between a N atom (labeled as ND, proton donor) in the amine group and a N atom (labeled as NA, proton acceptor) in P2VP. (c) Illustration of coarse-grained POSS with six amine groups and (d) eight amine groups; the blue sphere represents the POSS core and orange sites represent amine groups.

RESULTS AND DISCUSSION

Coarse-grained simulations of T_g of P2VP/NH_2-OPS nanocomposites indicated that the T_g enhancement depends on n_{amine} and the volume fraction of POSS, ϕ_{POSS}. In the simulation, we cooled down our systems with a constant cooling rate of $10^{-4}k_BT/\tau$ from 1.1 k_BT to 0.1 k_BT, which yields density−temperature curves (Figure S1). The T_g value was measured as the intersection of straight-line extrapolations from the glassy and liquid sections of the curve. Figure 2a shows the composition dependence of T_g on both ϕ_{POSS} and n_{amine}. In line with previous works, an increasing number of interacting sites between the polymer and POSS increases T_g of the composite.[7]

The T_g of P2VP/NH_2-OPS nanocomposites was also studied experimentally as a function of n_{amine} and ϕ_{POSS}, in good agreement with the trends observed in coarse-grained simulations. NH_2-OPS with a variable number of amines per POSS (n_{amine}) was synthesized according to a literature procedure.[35] Weakly entangled/unentangled P2VP (M_n = 30 kDa relative to polystyrene standards, $Đ$ = 1.16, M_e = 27 kDa[36]) was synthesized by reversible addition−fragmentation chain-transfer (RAFT) polymerization and loaded with NH_2-OPS via cocasting from tetrahydrofuran (THF) and subsequent annealing at 180 °C for 3 days under vacuum.[7,14,15] The effect of entanglements and molecular weight on the structure and dynamics of P2VP/POSS composites warrant future study but seem to be categorically different from the molecular weight effects on nanocomposites with larger fillers.[15,37,38] The experimentally achievable range of the average number of amines ($\langle n_{amine}\rangle$) was 5.7 to 7.3, as measured by electrospray ionization mass spectrometry (ESI-MS) (Table S1, Figure S2). The lower limit of n_{amine} was determined by the limited solubility, while the higher limit was determined by the highest conversion accessible in the reaction. ESI-MS revealed the exact distribution of molecular POSS species with different numbers of amines from which the average number in each sample was calculated (Figure 3). This distribution was sharpest for samples with high $\langle n_{amine}\rangle$ and considerably broadened as $\langle n_{amine}\rangle$ decreased across samples. The values of $\langle n_{amine}\rangle$ obtained from ESI-MS agreed well with those from proton nuclear magnetic resonance (^{1}H NMR) (Figure S5). Nanocomposite samples were prepared with

https://doi.org/10.1021/acs.macromol.2c00646
Macromolecules 2022, 55, 4891−4898

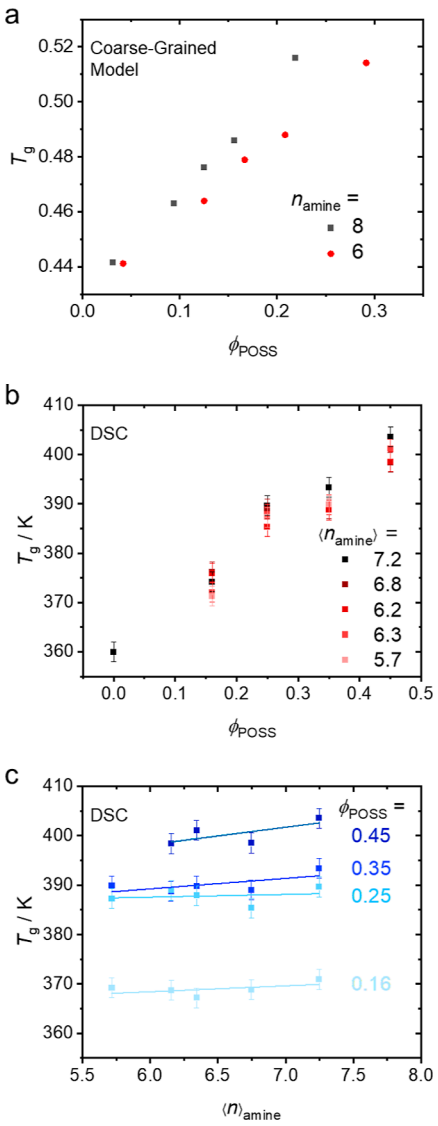

Figure 2. Plots of T_g vs the composition in P2VP/NH_2-OPS composites from (a) coarse-grained simulations and (b) DSC, with error bars corresponding to experimental uncertainty. Both results show a strong increase in T_g with OAPS loading, matching literature results. T_g also increases with n_{amine}, seen clearly in the simulation results, while the trend in the experimental result is less apparent due to instrumental uncertainty. Unloaded polymer is plotted at $\phi_{POSS} \cdot \langle n_{amine} \rangle = 0$. Data replotted to show the trend of T_g with $\langle n_{amine} \rangle$ are shown with linear fits to guide the eye for each value of ϕ_{POSS} (c).

$\langle n_{amine} \rangle$ = 5.7, 6.2, 6.3, 6.7, and 7.3 and ϕ_{POSS} = 0 (neat polymer), 0.16, 0.26, 0.35, and 0.45. After annealing, the dispersion of NH_2-OPS in the composite was checked by visual inspection and small-angle X-ray scattering (SAXS) (Figure S6).[7] All samples were found to have NH_2-OPS well dispersed in the polymer matrix, with the exception of the $\langle n_{amine} \rangle$ = 5.7, ϕ_{POSS} = 0.45 sample (the lowest number of amines and the highest NH_2-OPS loading), which was thus excluded from the analysis.

The glass transition temperature of each nanocomposite was measured by DSC (full data set in Figure S7). As expected, T_g increased monotonically with NH_2-OPS loading (ϕ_{POSS}), as shown in Figure 2b, and does not saturate at high loadings, suggesting that the polymer is essentially "all-interfacial"

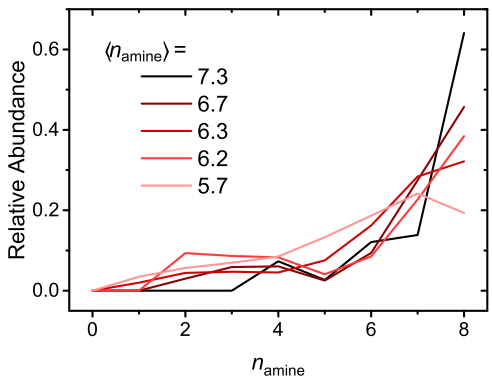

Figure 3. Distribution of the number of amines (n_{amine}) in the different NH_2-OPS products measured by ESI-MS.

without a distinct interfacial layer surrounding the nanoparticle.[34] We note that the trend of T_g with $\langle n_{amine} \rangle$ is less apparent compared to the results from coarse-grained simulations. This difference is rationalized by the high experimental uncertainty of the DSC T_g measurement, the distribution of n_{amine} in samples used for DSC, and the complexity of bond directionality not captured in the coarse-grained model. Nevertheless, both results are consistent with the hypothesis that T_g increases with the increasing number of interactions, that is, increasing n_{amine} (Figure 2c) and increasing ϕ_{POSS}.

Coarse-grained simulation and experimental measurements of T_g collapse when plotted against the product of ϕ_{POSS} and $\langle n_{amine} \rangle$, which is assumed to be proportional to the mole fraction of hydrogen bonding (f_{bonded}) according to our recent work (Figure 4 solid line).[7] This argument can naturally be extended to the P2VP/NH_2-OPS composite by assuming that the number of interactions is proportional to the number of amines.

$$f_{bonded} \propto \phi_{POSS} \cdot n_{amine} \tag{1}$$

f_{bonded} is then used as a component in the Fox equation with the glass transition temperature $T_{g,bonded}$, a fitting parameter conceptually equal to the T_g of a monomer that is hydrogen-bonded to POSS, and $T_{g,neat}$ is the T_g of the unloaded polymer.

$$\frac{1}{T_{g,composite}} = \frac{f_{bonded}}{T_{g,bonded}} + \frac{1 - f_{bonded}}{T_{g,neat}} \tag{2}$$

The data presented in Figure 4 are fitted to eqs 1 and 2 as illustrated in Figure S8. This result is also in qualitative agreement with theories which predict an approximately linear increase in T_g with the number of interactions in a homogeneous melt (Figure 4, dashed lines).[31−33]

In order to quantitively characterize the influence of H-bonds in coarse-grained simulations, we defined the second excessive entropy[39] S_{ex} with reference to the ideal gas

$$S_{ex} = -2\pi\rho_{matrix}\phi_{POSS}n_{amine}\int_0^\infty dr(g_{POSS\text{-}matrix}(r) \ln g_{POSS\text{-}matrix}(r) - g_{POSS\text{-}matrix}(r) + 1)r^2 \tag{3}$$

System entropy is defined as $S \simeq S_{id} + S_{ex}$, where $S_{ex} = 0$ represents the entropy of the ideal gas. In eq 3, ρ_{matrix} is the number density of POSS nanoparticles and $g_{poss\text{-}matrix}(r)$ represents the radial distribution function between the POSS center and matrix monomers. The results are plotted in Figure

https://doi.org/10.1021/acs.macromol.2c00646
Macromolecules 2022, 55, 4891−4898

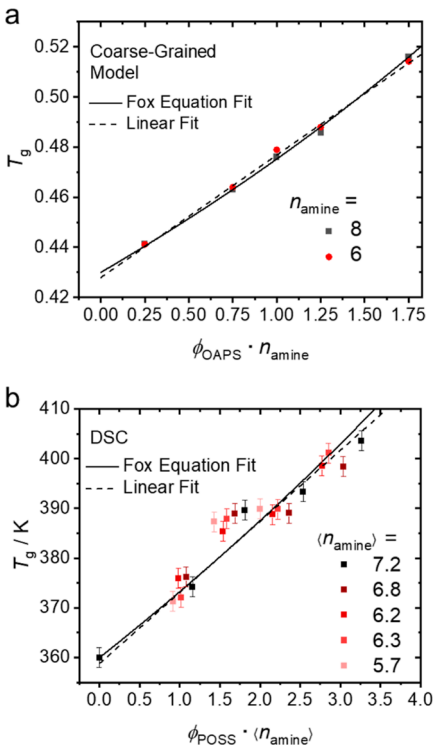

Figure 4. T_g of P2VP/NH_2-OPS composites from (a) coarse-grained simulations and (b) DSC, plotted vs the product of POSS loading and polymer/POSS bond site fractions with a fitting line according to eq 2 (Fox equation, solid lines) or a linear fit (dashed lines). The coarse-grained results collapse when plotted this way, and the experimental results agree reasonably well.

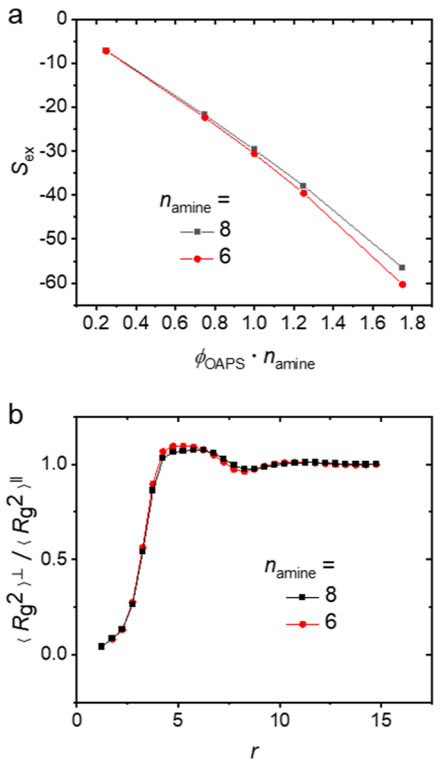

Figure 5. (a) Excess entropy in the composite via simulations also displays a collapse when plotted according to the product of filler loading and filler functionality. (b) Ratio of radial/tangent components of the squared radius of the gyration profile with respect to the POSS center at $\phi_{POSS} \times n_{amine} = 1.75$, the last point in (a).

5. For both $n_{amine} = 6$ and $n_{amine} = 8$ systems, the excessive entropy S_{ex} decreases linearly with respect to $\phi_{POSS} \times n_{amine}$. This demonstrates that entropy of matrix monomers decreases linearly with the increasing number of H-bonds; this result is intuitive that the total number of influenced monomers is proportional to the total number of H-bonds. Since the number of H-bonds is proportional to the number of donors and acceptors when the number of H-bonds is constant, that is, the same $\phi_{POSS} \times n_{amine}$ value in our simulations, the same S_{ex} can be expected.

However, POSS with eight NH_2 groups has stronger attractive hydrogen bonding interactions in total than that with six NH_2 groups. Therefore, matrix chains are more severely adsorbed in the vicinity of POSS in the system with eight NH_2 groups. In order to quantitatively characterize such differences in the adsorbed chain conformation, we calculated the radius of gyration tensors of chain segments which are 10 monomers long along the radial and tangential directions of the POSS surface

$$\langle R_g^2 \rangle^{\perp} := \left\langle \frac{1}{s^2} \sum_i \sum_{j>i} \left| r_{ij} \frac{r_{ij} \cdot (r_i + r_j)}{|r_{ij}||r_i + r_j|} \right| \right\rangle^2 \quad (4)$$

$$\langle R_g^2 \rangle^{\parallel} := \frac{1}{2} \left(\left\langle \frac{1}{s^2} \sum_i \sum_{j>i} |r_{ij}|^2 \right\rangle - \langle R_g^2 \rangle^{\perp} \right) \quad (5)$$

In eqs 4 and 5, r_i represents the position of ith monomer of the segment with a length of s and $r_{ij} := r_j - r_i$. Figure 5b shows the ratios between these two components with respect to the distance to the POSS center. Small values of this ratio at short distances ($r < 4$) to the POSS surface demonstrate a tangentially oriented chain conformation along the POSS surface. This value converges to 1 at positions far away from POSS, where the influence of POSS on chain conformation vanishes, and there are no differences in the radial and tangential components of the radius of gyration tensors. In addition, we see that for POSS with eight NH_2 groups, the ratio between the radial and tangential R_g components is noticeably smaller than that in the system with six NH_2 groups, demonstrating a stronger chain orientation surrounding POSS with eight NH_2 groups. Such a stronger chain orientation will cause a denser monomer packing in this interface region ($r < 4$), which is responsible for the lower entropy loss in S_{ex} with $n_{amine} = 8$ observed in Figure 5a.

In coarse-grained simulations, we simply modeled H-bonds as pairwise potentials; therefore, each amine group has the same probability to form H-bonds. However, the presence of neighboring bonding sites may influence the bonding probability due to configurational limitations.[40,41] In all-atom simulations, we had one POSS molecule presented in the system, and we analyzed the number of H-bonds per POSS molecule ($N_{H\text{-bond}}$) as a function of n_{amine} and temperature in a P2VP matrix (Figure 6a). $N_{H\text{-bond}}$ decreases substantially with temperature, decreasing by almost a factor of 2 in the temperature range studied (400 to 530 K) for both values of n_{amine}. Also, in line with assumptions used to construct the Fox equation fitting in Figure 4, the probability of hydrogen bond formation increases with the number of interaction sites in the nanocomposite (i.e., $N_{H\text{-bond}}$ increases with n_{amine}).

https://doi.org/10.1021/acs.macromol.2c00646
Macromolecules 2022, 55, 4891−4898

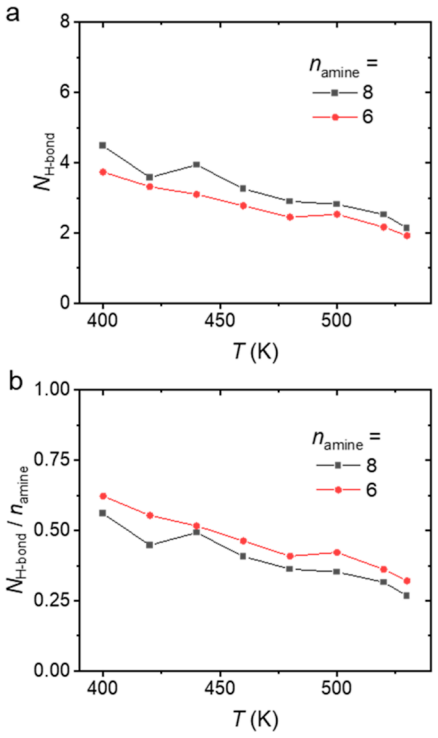

Figure 6. (a) Number of hydrogen bonds as a function of temperature and n_{amine} revealed by all-atom molecular dynamics simulations. There is a strong temperature dependence. (b) Fewer amines lead to fewer hydrogen bonds, but this decrease is less than linearly proportional to n_{amine}, indicating that the number of interactions between the polymer and filler is more complex than would be assumed by the random mixing argument.

However, the increase in $N_{H\text{-bond}}$ is less than proportional to the increase in n_{amine} (Figure 6b). In other words, when the number of amines on each POSS is lower, each individual amine has a higher probability of participating in a hydrogen bond, likely due to the chain frustration associated with bonding to neighboring amines. The nonlinearity between n_{amine} and $N_{H\text{-bond}}$ shows that our assumption of a uniform spatial distribution of monomers and POSS was not entirely accurate when the number of amines on NH_2-POSS changes, which justifies the weaker than expected trend observed in the experimentally observed trends in T_g versus ϕ_{POSS} times n_{amine} in Figure 3b. In other words, f_{bonded} has a more complex composition dependence than previously assumed. This effect is not observed in the coarse-grained model because the direction-specific nature of hydrogen bonding is not considered in our coarse-grained model.[40] As a whole, our results show that approximating f_{bonded} to be proportional to the number of polymer−POSS interactions is generally sufficient to match experimental observations; however, this assumption slightly overestimates the number of hydrogen bonding sites observed in simulations due to the greater configurational freedom present in nanocomposites with fewer interaction sites.

CONCLUSIONS

Through a combination of coarse-grained/all-atom simulations and experiments, we showed that the T_g enhancement effect of NH_2-OPS loaded in P2VP increases with the average number of amines present on POSS. Coarse-grained simulations suggested that the T_g enhancement can be explained by the excess interaction energy relative to the ideal gas state, which corresponds to the hydrogen bonding energy. Experimentally measured $T_g-\phi_{POSS}$ relationships of the composites with well-dispersed NH_2-POSS were consistent with those from the coarse-grained simulation, while they revealed a weaker increase in T_g with respect to the number of amines compared to the coarse-grained simulation results. These simulation and experimental results agreed with previous observations that T_g enhancement in polymer−POSS composites can be explained by the number of interactions between the two components.[7] These results are in agreement with prior simulations, experiments, and theories which show an approximately linear increase in T_g with interaction strength in nanocomposites and thin films,[26−31,42] provided that the polymer does not strongly adsorb to the surface to form a bound layer physically distinct from the free polymer matrix. This highlights an opportunity for future simulations to probe strongly interacting composite systems as the particle size increases from small, molecularly dispersed nanofillers to larger fillers with a distinct adsorbed layer.[6,34] All-atom molecular dynamics simulations provided detailed insights into the hydrogen bond interactions between NH_2-OPS and P2VP, which revealed that the number of interactions between the polymer and POSS did not exactly follow the previously assumed linear trend. The number of hydrogen bonds per POSS decreased with decreasing amine loading, but this decrease was not proportional to the number of amines, illustrating that the monomers are not in a perfect random distribution. Furthermore, these simulations revealed a strong temperature dependence on the number of hydrogen bonds in the system, decreasing by almost a factor of 2 over a 100 K increase in temperature. Our findings show that the number of interactions between the polymer and nanofiller, determined by the composition and temperature, can be a useful metric to describe effects such as T_g enhancement in polymer nanocomposites, particularly those with small fillers.

METHODS

Coarse-Grained Simulations. In coarse-grained simulations, a bead-spring model is adopted to describe polymer chains with a length of 200 type C beads, with nonbond 12−6 Lennard-Jones potentials

$$U_{lj}(r) = \begin{cases} 4\epsilon\left(\left(\frac{\sigma}{r-\Delta}\right)^{12} - \left(\frac{\sigma}{r-\Delta}\right)^{6}\right) & r < r_c \\ 0 & r \geq r \end{cases} \quad (6)$$

where σ is the bead length unit in our simulations and $\Delta := \frac{d_i + d_j}{2} - 1$, where d_i and d_j represent the diameters of particles i and j, respectively, and r_c is the cutoff distance of the nonbond potentials. The detailed parameters are shown in Table 1. Harmonic bonded potentials are adapted for bonded potentials, $U_{bond} = 0.5k(r - r_0)^2$ with $k = 1111$ and $r_0 = 1\sigma$.[43] The POSS nanoparticle is abstracted into a single sphere of type N with a diameter 4 times that of a

Table 1. Lennard-Jones Potential Table

pair	ϵ	r_c	Δ_{ij}
AA	1.0	$2^{1/6}\sigma$	0.0σ
AN	1.0	$2^{1/6}\sigma$	2.5σ
NN	1.0	$2^{1/6}\sigma$	3.0σ
AC	1.0	$2^{1/6}\sigma$	0.0σ
NC	1.0	$2^{1/6}\sigma$	2.5σ
CC	1.0	3.0σ	0.0σ

https://doi.org/10.1021/acs.macromol.2c00646
Macromolecules 2022, 55, 4891−4898

polymer bead with six or eight beads of type A representing NH_2 groups distributed evenly on the surface. Morse potentials

$$U_{morse}(r) = \begin{cases} D_0(\exp(-2\alpha(r - r_0)) - 2 \exp(-\alpha(r - r_0))) & r < r_c \\ 0 & r \geq r_c \end{cases} \quad (7)$$

are adapted for hydrogen bonds where the cutoff $r_c = 3.0\sigma$ is applied for all Morse pairs. Detailed parameters are shown in Table 2. We first

Table 2. Morse Potential Parameter Table

pair	D_0	α	r_0
AA	0.0	6.0	1.0σ
AN	0.0	6.0	1.0σ
NN	0.0	6.0	1.0σ
AC	3.0	6.0	1.5σ
NC	0.0	6.0	1.0σ
CC	0.0	6.0	1.0σ

perform NPT equilibration runs using Martyna−Tobias−Klein (MTK)[44] equations at reduced temperature $T = 1.0$ and pressure $p = 1.0$ after generating the systems; the equilibration runs stop when the mean-square-displacements of the center of mass of the polymer chains exceed $4R_g^2$ of the chains. After equilibration, all systems are annealed; the systems are first heated from $T = 1.0$ to $T = 1.5$ by $10^{-4}/\tau$ and then cooled from $T = 1.5$ to $T = 1.1$ by $10^{-4}/\tau$; after 5000τ equilibration at $T = 1.1$, the systems are finally cooled to $T = 0.1$ by $10^{-4}/\tau$. All simulations are performed using HOOMD-blue.[45]

All-Atom Simulations. Figure 1b shows one NH_2-OPS side group from all-atom molecular dynamics simulations. The hydrogen bond N···H−N is formed between nitrogen atoms (proton donor, labeled as ND) on OPS and nitrogen atoms (proton acceptor, labeled as NA) on P2VP. Octa(aminophenyl)silsesquinoxanes (OAPS) experiences strong attractive interactions due to hydrogen bonding with P2VP. The initial simulated system is constructed as follows: (1) first, the composite consisting of one OAPS and 120 P2VP with polymerization degree $N = 20$ is prepared at 530 K from our previous modeling work.[12] (2) To investigate how the number of amine groups on OAPS affects the formation of hydrogen bonds, we switch off the atomic charges of two "C−NH_2" (N, H, and C atoms labeled ND, HD, and CD, respectively) among the eight side groups in OAPS. Note that these two zero-charged "C−NH_2" are on the diagonal line of the OAPS Si−O cage, and the simulated system with this kind of OAPS is indicated as "Z6" otherwise "Z8", respectively. (3) Then, a stepwise cooling process with a cooling rate of −0.5 K ns^{-1} is applied from 530 to 400 K. (4) Finally, starting from the above discrete temperatures, a 200 ns *NPT* run is carried out to further equilibrate the systems. The trajectory of the last 100 ns is saved every 20 ps for data analysis. The number of hydrogen bonds is calculated and averaged from the trajectory. A hydrogen bond should meet the two following geometric criteria:[46] (1) the distance between HD and NA atoms should be less than 0.3 nm and (2) the ND−HD−HA angle should be larger than 130°. The Nośe−Hoover thermostat[47,48] is applied with a coupling time of 0.2 ps. The pressure is controlled by a Parrinello−Rahman barostat[49] with a coupling time of 1 ps. We use an OPLS-AA force field to describe the interactions in our simulated system, which is proven to be accurate and effective.[12,50] All the force field parameters can be found in our previous work.[12] A cutoff of 1.0 nm is used for calculating the van der Waals interactions, and the particle-mesh Ewald method is used to treat the electrostatic interactions. The energy and pressure calculations are corrected by the long-range dispersion. The integration of Newton's equations of motion is calculated by a leapfrog algorithm with a time step of 1 fs. All the atomistic simulations are carried out with GROMACS 5.1 software package.[51]

Materials. Octaphenyl silsesquioxane was purchased from Hybrid Plastics (Hattiesburg, MS, USA). Hexane, methanol, ethyl acetate, petroleum ether, fuming nitric acid, magnesium sulfate, ferric chloride, palladium on carbon (10%), and Celite 545 were purchased from Fisher Scientific (Waltham, MA, USA). Azobisisobutyronitrile (AIBN) and THF were purchased from Alfa Aesar (Haverhill, MA, USA). 2-Vinyl pyridine, basic alumina, calcium hydride, and hydrazine hydrate were purchased from Acros Organics (Fair Lawn, NJ, USA). Ethyl 2-(phenylcarbonothioylthio)-2-phenylacetate was purchased from Sigma-Aldrich (St. Louis, MO, USA). AIBN was recrystallized in methanol. 2-Vinyl pyridine was purified by passing through a column of basic alumina to remove the inhibitor. Anisole was dried over calcium hydride. All other materials were used as received.

NH_2-OPS Synthesis. NH_2-OPS was synthesized with slight modifications according to a recent literature procedure.[35,52−54] Nitric acid and acetic anhydride were added from separate addition funnels dropwise to a dispersion of OPS in dichloromethane, with a 5 g basis of OPS. The reaction flask was kept at 25 °C for times ranging from 15 to 180 min after addition of reagents over 5 min. The different reaction times correspond to the extent of nitration of OPS (Figure S3). The resultant NO_2-OPS was precipitated from the reaction solution in cold water before rotovapping to remove dichloromethane. The product was filtered to remove NO_2-OPS and rinsed thoroughly with concentrated sodium bicarbonate solution and water. The product was then dissolved in THF and precipitated into methanol before drying. NO_2-OPS was reduced to NH_2-OPS with hydrazine hydrate as an in situ hydrogen source with a ferric chloride catalyst, 5% Pd/C catalyst, and THF solvent reflux at 60 °C according to literature procedures (Figure S4).[52]

P2VP Synthesis. P2VP was synthesized via RAFT polymerization (Figures S9 and S10).[55] 20 g of 2 vinyl-pyridine was added to a 250 mL round-bottom flask with 15 mL of anisole. Ethyl 2-(phenylcarbonothioylthio)-2-phenylacetate was used as the RAFT chain-transfer agent (CTA), with AIBN as the initiator. Reagents were added at a 300:4:1 molar ratio of monomers to CTA to AIBN. The reaction was degassed with nitrogen for 30 min and then heated to 70 °C for 18 h before quenching at 0 °C for 30 min and precipitating in hexane three times.

Gel Permeation Chromatography. The molecular weight and dispersity of P2VP was characterized by gel permeation chromatography (GPC) using a mobile phase of dimethylformamide with a 0.01 M lithium chloride salt at 50 °C relative to a polystyrene standard. The GPC instrument consisted of an Agilent Technologies 1260 Infinity, fitted with a Gel 5 μm guard column, a PL Gel 5 μm mix D 1° column, and a PL Gel 5 μm Mix C 1° column. Samples were run at a flow rate of 1 mL/min using toluene as the flow rate marker.

Nuclear Magnetic Resonance. NMR measurements were taken on a Bruker 500 500MHz NMR instrument with cryoprobe attachments in solutions of acetone-d_6 at concentrations of 50 mg/mL.

Electrospray Ionization Mass Spectrometry. ESI time-of-flight MS was performed on a Bruker MicrOTOF ESI-TOF mass spectrometer at the University of Massachusetts Mass Spectrometry Core Facility. POSS samples were diluted to ∼10 μM with 1 mM formic acid in an acetonitrile/water (80:20 by weight) solution before injection.

Nanocomposite Sample Preparation. Nanocomposites were prepared by cocasting following modified literature procedures.[7,14,15] A total of 200 mg of P2VP and OPS-NH_2 was dissolved in 10 mL of THF at different weight ratios. The solvent was allowed to evaporate overnight at room temperature and atmospheric pressure before being placed in a vacuum oven <100 mTorr at 120 °C for 36 h to remove all remaining solvent. The samples were then melt-cast in polytetrafluoroethylene vials in a vacuum oven at ∼10^{-6} Torr at 180 °C for 3 days.

Small-Angle X-ray Scattering. Scattering measurements were performed on a SAXSLAB GANESHA small-/wide-angle X-ray scattering instrument. The source was Cu Kα 0.154 nm with a beam area of approximately 0.1 mm^2. All measurements were performed in transmission geometry on a nanocomposite powder sample 1 mm thick between layers of polyimide tape. Results are

https://doi.org/10.1021/acs.macromol.2c00646
Macromolecules 2022, 55, 4891−4898

reported as relative intensities on an arbitrary scale. SAXS measurements were acquired over 10 min.

Differential Scanning Calorimetry. Heat capacity versus temperature measurements were taken on a TA Instruments Q20 differential scanning calorimeter at a heating/cooling rate of 10 °C/min under nitrogen after annealing at 200 °C for 5 min. T_g is reported as the midpoint of the heat capacity inflection point upon second heating. Typical sample weights were ∼2 mg.

■ ASSOCIATED CONTENT

Supporting Information

The Supporting Information is available free of charge at https://pubs.acs.org/doi/10.1021/acs.macromol.2c00646.

Temperature−density curves from coarse-grained simulations, ESI-MS results of NH_2-OPS, ^{1}H NMR spectra of NO_2-OPS and NH_2-OPS, comparison of n_{amine} measured by ESI-MS and ^{1}H NMR, SAXS profiles of selected nanocomposites, DSC results of nanocomposites, fitting data to the modified Fox equation, and details of P2VP synthesis (PDF)

■ AUTHOR INFORMATION

Corresponding Authors

Hu-Jun Qian − *State Key Laboratory of Supramolecular Structure and Materials, College of Chemistry, Jilin University, Changchun 130021, China;* orcid.org/0000-0001-8149-8776; Email: hjqian@jlu.edu.cn

Reika Katsumata − *Department of Polymer Science and Engineering, University of Massachusetts Amherst, Amherst, Massachusetts 01003, United States;* orcid.org/0000-0003-3119-9385; Email: rkatsumata@umass.edu

Authors

Walter W. Young − *Department of Polymer Science and Engineering, University of Massachusetts Amherst, Amherst, Massachusetts 01003, United States*

Rui Shi − *State Key Laboratory of Supramolecular Structure and Materials, College of Chemistry, Jilin University, Changchun 130021, China*

Xiang-Meng Jia − *State Key Laboratory of Supramolecular Structure and Materials, College of Chemistry, Jilin University, Changchun 130021, China*

Complete contact information is available at: https://pubs.acs.org/10.1021/acs.macromol.2c00646

Author Contributions

W.W.Y., R.S., and X.-M.J. contributed equally. All authors have given approval to the final version of the manuscript.

Notes

The authors declare no competing financial interest.

■ ACKNOWLEDGMENTS

H.J.Q. and R.S. acknowledge the support form the National Natural Science Foundation of China (grant nos. 21873040 and 22103028). R.K. acknowledges the support of the NSF CAREER Award DMR # 2046606. We thank H Henning Winter for use of the differential scanning calorimeter. For the collection of ESI-MS data, the authors acknowledge Stephen J Eyles and the University of Massachusetts Mass Spectrometry Core Facility, RRID:SCR_019063. The authors acknowledge the UMass Amherst Nuclear Magnetic Resonance Facility and the UMass Amherst Gel Permeation Chromatography Facility.

■ REFERENCES

(1) Kumar, S. K.; Benicewicz, B. C.; Vaia, R. A.; Winey, K. I. 50th Anniversary Perspective: Are Polymer Nanocomposites Practical for Applications? *Macromolecules* **2017**, *50*, 714−731.

(2) Cheng, S.; Carroll, B.; Lu, W.; Fan, F.; Carrillo, J.-M. Y.; Martin, H.; Holt, A. P.; Kang, N.-G.; Bocharova, V.; Mays, J. W.; Sumpter, B. G.; Dadmun, M.; Sokolov, A. P. Interfacial Properties of Polymer Nanocomposites: Role of Chain Rigidity and Dynamic Heterogeneity Length Scale. *Macromolecules* **2017**, *50*, 2397−2406.

(3) Lin, E. Y.; Frischknecht, A. L.; Winey, K. I.; Riggleman, R. A. Effect of Surface Properties and Polymer Chain Length on Polymer Adsorption in Solution. *J. Chem. Phys.* **2021**, *155*, 034701.

(4) Zheng, Z.; Li, F.; Liu, J.; Pastore, R.; Raos, G.; Wu, Y.; Zhang, L. Effects of Chemically Heterogeneous Nanoparticles on Polymer Dynamics: Insights from Molecular Dynamics Simulations. *Soft Matter* **2018**, *14*, 1219−1226.

(5) Trazkovich, A. J.; Wendt, M. F.; Hall, L. M. Effect of Copolymer Sequence on Local Viscoelastic Properties near a Nanoparticle. *Macromolecules* **2019**, *52*, 513−527.

(6) Buitrago, C. F.; Pressly, J. F.; Gordon, P. A.; Natarajan, B.; Winey, K. I.; Natarajan, B.; Winey, I. Creep Attenuation in Glassy Polymer Nanocomposites with Variable Polymer−Nanoparticle Interactions. *Soft Matter* **2020**, *16*, 8912−8924.

(7) Young, W. W.; Saez, J. P.; Katsumata, R. Rationalizing the Composition Dependence of Glass Transition Temperatures in Amorphous Polymer/POSS Composites. *ACS Macro Lett.* **2021**, *10*, 1404−1409.

(8) Voylov, D. N.; Holt, A. P.; Doughty, B.; Bocharova, V.; Meyer, H. M.; Cheng, S.; Martin, H.; Dadmun, M.; Kisliuk, A.; Sokolov, A. P. Unraveling the Molecular Weight Dependence of Interfacial Interactions in Poly(2-Vinylpyridine)/Silica Nanocomposites. *ACS Macro Lett.* **2017**, *6*, 68−72.

(9) Cheng, S.; Bocharova, V.; Belianinov, A.; Xiong, S.; Kisliuk, A.; Somnath, S.; Holt, A. P.; Ovchinnikova, O. S.; Jesse, S.; Martin, H.; Etampawala, T.; Dadmun, M.; Sokolov, A. P. Unraveling the Mechanism of Nanoscale Mechanical Reinforcement in Glassy Polymer Nanocomposites. *Nano Lett.* **2016**, *16*, 3630−3637.

(10) Bocharova, V.; Genix, A.-C.; Carrillo, J.-M. Y.; Kumar, R.; Carroll, B.; Erwin, A.; Voylov, D.; Kisliuk, A.; Wang, Y.; Sumpter, B. G.; Sokolov, A. P. Addition of Short Polymer Chains Mechanically Reinforces Glassy Poly(2-Vinylpyridine)−Silica Nanoparticle Nanocomposites. *ACS Appl. Nano Mater.* **2020**, *3*, 3427−3438.

(11) Zhou, Y.; Schweizer, K. S. Theory for the Elementary Time Scale of Stress Relaxation in Polymer Nanocomposites. *ACS Macro Lett.* **2022**, *11*, 199−204.

(12) Jia, X.-M.; Qian, H.-J.; Lu, Z.-Y. The Interfacial Structure and Dynamics in a Polymer Nanocomposite Containing Small Attractive Nanoparticles: A Full Atomistic Molecular Dynamics Simulation Study. *Phys. Chem. Chem. Phys.* **2020**, *22*, 11400−11408.

(13) Jouault, N.; Kumar, S. K.; Smalley, R. J.; Chi, C.; Moneta, R.; Wood, B.; Salerno, H.; Melnichenko, Y. B.; He, L.; Guise, W. E.; Hammouda, B.; Crawford, M. K. Do Very Small POSS Nanoparticles Perturb S-PMMA Chain Conformations? *Macromolecules* **2018**, *51*, 5278−5293.

(14) Cheng, S.; Xie, S.-J.; Carrillo, J.-M. Y.; Carroll, B.; Martin, H.; Cao, P.-F.; Dadmun, M. D.; Sumpter, B. G.; Novikov, V. N.; Schweizer, K. S.; Sokolov, A. P. Big Effect of Small Nanoparticles: A Shift in Paradigm for Polymer Nanocomposites. *ACS Nano* **2017**, *11*, 752−759.

(15) Bailey, E. J.; Griffin, P. J.; Composto, R. J.; Winey, K. I. Multiscale Dynamics of Small, Attractive Nanoparticles and Entangled Polymers in Polymer Nanocomposites. *Macromolecules* **2019**, *52*, 2181−2188.

(16) Emamy, H.; Kumar, S. K.; Starr, F. W. Diminishing Interfacial Effects with Decreasing Nanoparticle Size in Polymer-Nanoparticle Composites. *Phys. Rev. Lett.* **2018**, *121*, 207801.

(17) Song, Y.; Zheng, Q. Size-Dependent Linear Rheology of Silica Filled Poly(2-Vinylpyridine). *Polymer* **2017**, *130*, 74−78.

(18) Khan, R. A. A.; Qi, H.-K.; Huang, J.-H.; Luo, M.-B. A Simulation Study on the Effect of Nanoparticle Size on the Glass Transition Temperature of Polymer Nanocomposites. *Soft Matter* **2021**, *17*, 8095−8104.
(19) Cheng, S.; Sokolov, A. P. Correlation between the Temperature Evolution of the Interfacial Region and the Growing Dynamic Cooperativity Length Scale. *J. Chem. Phys.* **2020**, *152*, 094904.
(20) Romo-Uribe, A.; Reyes-Mayer, A.; Paredes-Pérez, M.; Lichtenhan, J.; Yañez-Lino, M.; Sarmiento-Bustos, E. POSS Driven Chain Disentanglements, Decreased the Melt Viscosity and Reduced O2 Transmission in Polyethylene. *Polymer* **2019**, *165*, 61−71.
(21) Zhang, X.; Zhao, S.; Xin, Z. The Chain Dis-Entanglement Effect of Polyhedral Oligomeric Silsesquioxanes (POSS) on Ultra-High Molecular Weight Polyethylene (UHMWPE). *Polymer* **2020**, *202*, 122631.
(22) Raftopoulos, K. N.; Pielichowski, K. Segmental Dynamics in Hybrid Polymer/POSS Nanomaterials. *Prog. Polym. Sci.* **2016**, *52*, 136−187.
(23) Kopesky, E. T.; Haddad, T. S.; McKinley, G. H.; Cohen, R. E. Miscibility and Viscoelastic Properties of Acrylic Polyhedral Oligomeric Silsesquioxane−Poly(Methyl Methacrylate) Blends. *Polymer* **2005**, *46*, 4743−4752.
(24) Kuo, S.-W.; Lin, H.-C.; Huang, W.-J.; Huang, C.-F.; Chang, F.-C. Hydrogen Bonding Interactions and Miscibility between Phenolic Resin and Octa(Acetoxystyryl) Polyhedral Oligomeric Silsesquioxane (AS-POSS) Nanocomposites. *J. Polym. Sci., Part B: Polym. Phys.* **2006**, *44*, 673−686.
(25) Fox, T. G. Influence of Diluent and of Copolymer Composition on the Glass Temperature of a Polymer System. *Bull. Am. Phys. Soc.* **1956**, *1*, 123.
(26) Fryer, D. S.; Peters, R. D.; Kim, E. J.; Tomaszewski, J. E.; de Pablo, J. J.; Nealey, P. F.; White, C. C.; Wu, W.-l. Dependence of the Glass Transition Temperature of Polymer Films on Interfacial Energy and Thickness. *Macromolecules* **2001**, *34*, 5627−5634.
(27) Natarajan, B.; Li, Y.; Deng, H.; Brinson, L. C.; Schadler, L. S. Effect of Interfacial Energetics on Dispersion and Glass Transition Temperature in Polymer Nanocomposites. *Macromolecules* **2013**, *46*, 2833−2841.
(28) Chen, F.; Clough, A.; Reinhard, B. M.; Grinstaff, M. W.; Jiang, N.; Koga, T.; Tsui, O. K. C. Glass Transition Temperature of Polymer−Nanoparticle Composites: Effect of Polymer−Particle Interfacial Energy. *Macromolecules* **2013**, *46*, 4663−4669.
(29) Torres, J. A.; Nealey, P. F.; de Pablo, J. J. Molecular Simulation of Ultrathin Polymeric Films near the Glass Transition. *Phys. Rev. Lett.* **2000**, *85*, 3221−3224.
(30) Starr, F. W.; Schrøder, T. B.; Glotzer, S. C. Molecular Dynamics Simulation of a Polymer Melt with a Nanoscopic Particle. *Macromolecules* **2002**, *35*, 4481−4492.
(31) Lang, R. J.; Merling, W. L.; Simmons, D. S. Combined Dependence of Nanoconfined T_g on Interfacial Energy and Softness of Confinement. *ACS Macro Lett.* **2014**, *3*, 758−762.
(32) Stukalin, E. B.; Douglas, J. F.; Freed, K. F. Application of the Entropy Theory of Glass Formation to Poly(α-Olefins). *J. Chem. Phys.* **2009**, *131*, 114905.
(33) Ghosh, A.; Samanta, S.; Ge, S.; Sokolov, A. P.; Schweizer, K. S. Influence of Attractive Functional Groups on the Segmental Dynamics and Glass Transition in Associating Polymers. *Macromolecules* **2022**, *55*, 2345.
(34) Starr, F. W.; Douglas, J. F.; Meng, D.; Kumar, S. K. Bound Layers "Cloak" Nanoparticles in Strongly Interacting Polymer Nanocomposites. *ACS Nano* **2016**, *10*, 10960−10965.
(35) Wu, Y.-w.; Liu, L.-c.; Yang, R.-j.; Zhang, W.-c. Synthesis and Characterization of Low-Functional Nitrated and Aminated Octa-(Phenyl) Silsesquioxane. *ChemistrySelect* **2019**, *4*, 2941−2948.
(36) Jouault, N.; Moll, J. F.; Meng, D.; Windsor, K.; Ramcharan, S.; Kearney, C.; Kumar, S. K. Bound Polymer Layer in Nanocomposites. *ACS Macro Lett.* **2013**, *2*, 371−374.
(37) Yamamoto, U.; Carrillo, J.-M. Y.; Bocharova, V.; Sokolov, A. P.; Sumpter, B. G.; Schweizer, K. S. Theory and Simulation of Attractive Nanoparticle Transport in Polymer Melts. *Macromolecules* **2018**, *51*, 2258−2267.
(38) Carroll, B.; Bocharova, V.; Carrillo, J.-M. Y.; Kisliuk, A.; Cheng, S.; Yamamoto, U.; Schweizer, K. S.; Sumpter, B. G.; Sokolov, A. P. Diffusion of Sticky Nanoparticles in a Polymer Melt: Crossover from Suppressed to Enhanced Transport. *Macromolecules* **2018**, *51*, 2268−2275.
(39) Dyre, J. C. Perspective: Excess-Entropy Scaling. *J. Chem. Phys.* **2018**, *149*, 210901.
(40) Jayaraman, A. 100th Anniversary of Macromolecular Science Viewpoint: Modeling and Simulation of Macromolecules with Hydrogen Bonds: Challenges, Successes, and Opportunities. *ACS Macro Lett.* **2020**, *9*, 656−665.
(41) Kulshreshtha, A.; Modica, K. J.; Jayaraman, A. Impact of Hydrogen Bonding Interactions on Graft−Matrix Wetting and Structure in Polymer Nanocomposites. *Macromolecules* **2019**, *52*, 2725−2735.
(42) Hanakata, P. Z.; Pazmiño Betancourt, B. A.; Douglas, J. F.; Starr, F. W. A Unifying Framework to Quantify the Effects of Substrate Interactions, Stiffness, and Roughness on the Dynamics of Thin Supported Polymer Films. *J. Chem. Phys.* **2015**, *142*, 234907.
(43) Shi, R.; Qian, H.-J.; Lu, Z.-Y. Interfacial Tuning of the Cavitation and Strain-Softening Behavior of Polymer/Nanoparticle Composites in the Glassy State. *Macromolecules* **2019**, *52*, 7353−7360.
(44) Martyna, G. J.; Tobias, D. J.; Klein, M. L. Constant Pressure Molecular Dynamics Algorithms. *J. Chem. Phys.* **1994**, *101*, 4177−4189.
(45) Anderson, J. A.; Glaser, J.; Glotzer, S. C. HOOMD-Blue: A Python Package for High-Performance Molecular Dynamics and Hard Particle Monte Carlo Simulations. *Comput. Mater. Sci.* **2020**, *173*, 109363.
(46) Eslami, H.; Rahimi, M.; Müller-Plathe, F. Molecular Dynamics Simulation of a Silica Nanoparticle in Oligomeric Poly(Methyl Methacrylate): A Model System for Studying the Interphase Thickness in a Polymer−Nanocomposite via Different Properties. *Macromolecules* **2013**, *46*, 8680−8692.
(47) Nosé, S. A Molecular Dynamics Method for Simulations in the Canonical Ensemble. *Mol. Phys.* **1984**, *52*, 255−268.
(48) Hoover, W. G. Canonical Dynamics: Equilibrium Phase-Space Distributions. *Phys. Rev. A: At., Mol., Opt. Phys.* **1985**, *31*, 1695−1697.
(49) Parrinello, M.; Rahman, A. Polymorphic Transitions in Single Crystals: A New Molecular Dynamics Method. *J. Appl. Phys.* **1981**, *52*, 7182−7190.
(50) Caputo, S.; De Nicola, A.; Donati, G.; David, A.; Raos, G.; Milano, G. All-Atom Model of Atactic 2-Vinyl Pyridine Polymer: Structural Properties Investigation by Molecular Dynamics Simulations. *J. Electrochem. Soc.* **2019**, *166*, B3309.
(51) Hess, B.; Kutzner, C.; van der Spoel, D.; Lindahl, E. GROMACS 4: Algorithms for Highly Efficient, Load-Balanced, and Scalable Molecular Simulation. *J. Chem. Theory Comput.* **2008**, *4*, 435−447.
(52) Fan, H.; Yang, R.; Li, D. Synthesis Improvement and Characterization of Polyhedral Oligomeric Octa(Aminophenyl)-Silsesquioxane. *Acta Chim. Sin.* **2012**, *70*, 429.
(53) Zhang, J.; Xu, R.-W.; Yu, D.-S. A Novel and Facile Method for the Synthesis of Octa(Aminophenyl)Silsesquioxane and Its Nanocomposites with Bismaleimide-Diamine Resin. *J. Appl. Polym. Sci.* **2007**, *103*, 1004−1010.
(54) Tamaki, R.; Tanaka, Y.; Asuncion, M. Z.; Choi, J.; Laine, R. M. Octa(Aminophenyl)Silsesquioxane as a Nanoconstruction Site. *J. Am. Chem. Soc.* **2001**, *123*, 12416−12417.
(55) Bryson, K. C. *Controlling the Assembly of Nanoparticles in Polymer Blends*, University of Massachusettes Amherst, 2016.

https://doi.org/10.1021/acs.macromol.2c00646
Macromolecules 2022, 55, 4891−4898